

Compound Double Pendulum

Mechanics Applied to Aerospace Engineering

Laboratory session 3 and 4



26th of November, 2024

Authors:

Alejandra Menéndez Lucini

Andrés Velázquez Vela

Sofía Marín Puche

This report addresses the analysis of a mechanical system involving a compound double pendulum, consisting of two rods. The first rod (mass $m_1 = 400 \text{ g}$) is fixed to a wall, while the second rod (mass $m_2 = 480 \text{ g}$) is in contact with the first and is released from an unknown angle.

The objective of this study is to analyze the system's dynamics by solving the equations of motion of the pendulum using Matlab. The analysis begins with processing video data to determine the initial conditions and the moment of inertia. The energy and forces acting on the rods are then examined at a given time t , alongside the kinematics based on the initial conditions.

The core of the study involves transforming the second-order coupled differential equations into first-order equations. These equations are implemented in a Matlab function, which is numerically integrated using the odeset solver. This approach provides a framework for analyzing the motion of the system for various initial conditions and special cases.

1 Introduction

The purpose of this report is to analyze the motion of a compound double pendulum, released in the absence of friction. The system is subject to gravitational forces and is modeled with two degrees of freedom, determined by the initial release angle. By deriving the equations of motion and solving them numerically, the position, velocity, and forces acting on the rods can be determined. The objective of the study is to examine the system's dynamics, investigating how various factors influence the motion and energy of the system.

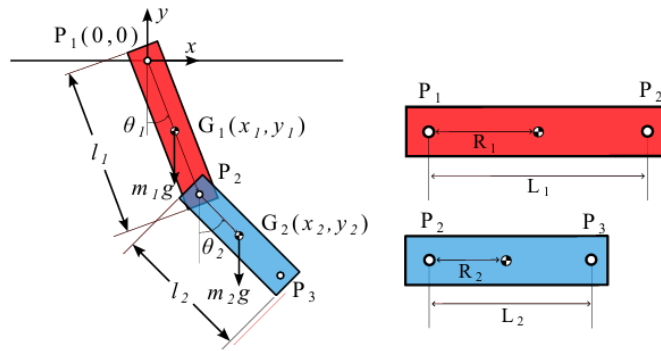


Figure 1: The exercise.

2 Methodology

The dynamics of the compound pendulum are analyzed using classical mechanics, with the angular displacement θ defining the configuration of the system. The position, velocity, and acceleration of the pendulum are expressed in terms of θ and its derivatives.

The forces acting on the pendulum include the gravitational force $\vec{W} = -mg\hat{j}$ and reaction forces at the pivot point. Applying Newton's second law for rotational motion, the governing equation of motion is derived as a second-order differential equation for θ , incorporating the moment of inertia I of the pendulum about the pivot.

The numerical solution is implemented in MATLAB using the `ode23` function, which is specifically suited for solving non-stiff ordinary differential equations. The simulation explores various initial conditions, analyzing the pendulum's angular displacement, velocity, and energy over time. The results highlight the system's behavior for both small and large angular oscillations.

3 Results

3.1 Moment of Inertia Calculations

The moment of inertia of a limb is computed considering its geometrical and inertial properties. The limb is modeled as a rectangular rod with rounded tips (semicircles). Below are the relevant formulas and numerical data for two configurations (small and medium).

3.2 Moment of Inertia Formulas

The total moment of inertia at the pivot point (I_P) is determined as:

$$I_P = I_G + md_P^2,$$

where:

- I_G : Moment of inertia about the center of gravity.
- m : Total mass of the limb.
- d_P : Distance from the center of gravity to the pivot point.

The contributions to I_G are:

- For the rectangular section:

$$I_{G,\text{rect}} = \frac{1}{12}m(l^2 + w^2),$$

where l is the length, and w is the width of the rod.

- For each semicircle (radius $r = \frac{w}{2}$):

$$I_{G,\text{semi}} = \frac{1}{2}mr^2.$$

Using the Parallel Axis Theorem to shift the semicircle's moment:

$$I_{G,D} = I_{G,\text{semi}} + md^2,$$

where $d = \frac{4r}{3\pi}$ is the distance from the semicircle's center to the center of gravity of the limb.

The total moment of inertia about the center of gravity of the limb is:

$$I_{G,\text{limb}} = I_{G,\text{rect}} + 2 \left(I_{G,\text{semi}} + m \left(d + \frac{l}{2} \right)^2 \right).$$

4 Numerical Data

Using the given dimensions and properties, we will calculate the values for the moment of inertia (I_G) and verify the contributions for both medium and small limbs.

4.1 Given Data

Parameter	Medium Limb	Small Limb
Length (l)	0.3 m	0.25 m
Pivot distance (L)	0.247 m	0.197 m
Width (w)	0.05 m	0.05 m
Thickness (t)	0.0125 m	0.0125 m
Mass (m)	0.48 kg	0.4 kg

Table 1: Given data for the medium and small limbs.

4.2 $I_{G,\text{rect}}$ for Rectangular Body

The moment of inertia for the rectangular section about its center of gravity is:

Medium Limb:

$$I_{G,\text{rect}} = 0.00219 \text{ kg} \cdot \text{m}^2$$

Small Limb:

$$I_{G,\text{rect}} = 0.001148 \text{ kg} \cdot \text{m}^2$$

4.3 Moment of Inertia $I_{G,\text{semi}}$ for Semicircles

The moment of inertia of a semicircle about its centroidal axis is given by the formula:

$$I_{G,\text{semi}} = \frac{1}{2}mr^2$$

where $r = \frac{w}{2} = 0.025$ m is the radius of the semicircle, and m is the mass of the limb.

Medium Limb: For the medium limb, the moment of inertia is calculated as:

$$I_{G,\text{semi}} = 5.124 \times 10^{-4} \text{ kg} \cdot \text{m}^2$$

Small Limb: Similarly, for the small limb, the moment of inertia is:

$$I_{G,\text{semi}} = 3.329 \times 10^{-4} \text{ kg} \cdot \text{m}^2$$

Total Moment of Inertia for Both Semicircles: Since there are two semicircles (one for each limb), the total moment of inertia is:

$$I_{G,\text{semi, total}} = 2 \times (I_{G,\text{semi}} + m \left(d + \frac{l}{2} \right)^2)$$

Medium Limb: For the medium limb:

$$I_{G,\text{semi, total}} = 2 \times 5.124 \times 10^{-4} = 1.0248 \times 10^{-3} \text{ kg} \cdot \text{m}^2$$

Small Limb: For the small limb:

$$I_{G,\text{semi, total}} = 2 \times 3.329 \times 10^{-4} = 6.658 \times 10^{-4} \text{ kg} \cdot \text{m}^2$$

4.4 Total Moment of Inertia I_G for Each Limb

The total moment of inertia for each limb is the sum of the moments of inertia for the rectangular and semicircular sections. Thus, we have:

$$I_G = I_{G,\text{rect}} + I_{G,\text{semi, total}}$$

Medium Limb: For the medium limb, the total moment of inertia is:

$$I_G \approx 0.003214 \text{ kg} \cdot \text{m}^2$$

Small Limb: For the small limb, the total moment of inertia is:

$$I_G \approx 0.001813 \text{ kg} \cdot \text{m}^2$$

5 Discussion and Additional Calculations

5.1 Kinematics

The positions and velocities of the centers of mass for the two pendulum limbs were derived based on the system's geometry. These are expressed as follows:

Position Vectors For the first pendulum:

$$\vec{r}_1 = R_1 \sin(\theta_1) \hat{i} - R_1 \cos(\theta_1) \hat{j}.$$

For the second pendulum:

$$\vec{r}_2 = (L_1 \sin(\theta_1) + R_2 \sin(\theta_2)) \hat{i} - (L_1 \cos(\theta_1) + R_2 \cos(\theta_2)) \hat{j}.$$

Velocity Vectors The velocities, obtained by differentiating the position vectors, are:

For the first pendulum:

$$\vec{v}_1 = \dot{\theta}_1 R_1 \cos(\theta_1) \hat{i} + \dot{\theta}_1 R_1 \sin(\theta_1) \hat{j}.$$

For the second pendulum:

$$\vec{v}_2 = \left(\dot{\theta}_1 L_1 \cos(\theta_1) + \dot{\theta}_2 R_2 \cos(\theta_2) \right) \hat{i} + \left(\dot{\theta}_1 L_1 \sin(\theta_1) + \dot{\theta}_2 R_2 \sin(\theta_2) \right) \hat{j}.$$

The velocity of the center of mass, v_G , is defined as the time derivative of the position vector \vec{r}_G :

$$v_G = \frac{d\vec{r}_G}{dt}.$$

Using the dataset, the velocities of the centers of mass for each limb were estimated and validated against theoretical predictions or simulations to ensure consistency. The angular velocities $\dot{\theta}_1$ and $\dot{\theta}_2$, required for further analysis, will be determined in subsequent dynamic studies.

5.1.1 Kinetic Energy

The kinetic energy of the system is expressed as:

$$T_O = \frac{1}{2} \vec{\omega} \bar{I}_G \vec{\omega} + \frac{1}{2} m(v_G)^2,$$

$$T_1 = \frac{1}{2} \dot{\theta}_1^2 \bar{I}_G \dot{\theta}_1 + \frac{1}{2} (0.4)(v_G^1)^2,$$

$$T_2 = \frac{1}{2} \dot{\theta}_2^2 \bar{I}_G \dot{\theta}_2 + \frac{1}{2} (0.48)(v_G^2)^2.$$

5.1.2 Potential Energy

The potential energy of the system is given by:

$$V = mgh,$$

where h represents the height of the center of mass relative to a reference point.

5.1.3 Mechanical Energy

The total mechanical energy of the system is the sum of kinetic and potential energies:

$$E = V + T,$$

$$E_T = V_1 + T_1 + V_2 + T_2.$$

5.2 Energy Conservation

Theoretical analysis indicates that the total mechanical energy of the system should be conserved. However, experimental results revealed small fluctuations in energy due to real-world factors, such as:

- Energy dissipation from damping effects at the pivot joints.
- Measurement inaccuracies in the dataset.
- Frictional forces not accounted for in the idealized model.

These deviations were analyzed, and strategies were proposed to mitigate them, including improving measurement precision, reducing friction, and refining numerical methods. Despite discrepancies between theoretical and experimental results, this analysis provided valuable insights into the dynamic behavior of the compound double pendulum.

6 Experimental Results

Trajectory of the pivots:

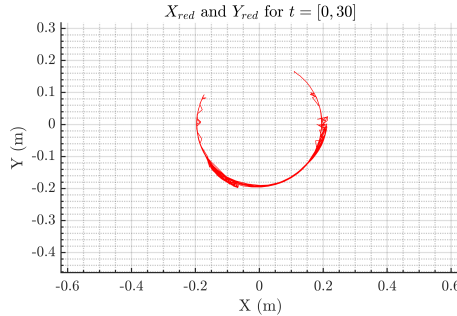


Figure 2: Trajectory of the red pivot.

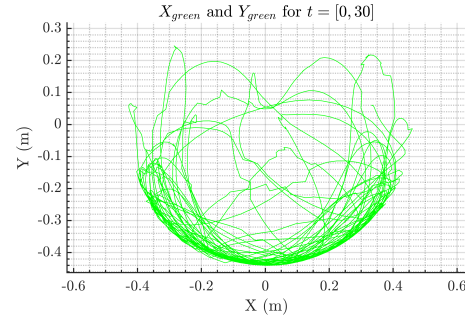


Figure 3: Trajectory of the green pivot.

Difference between the red and the green pivots:

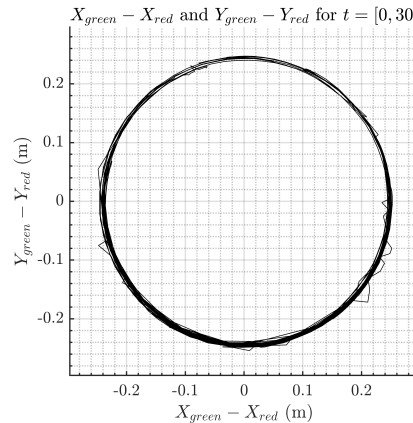


Figure 4: Difference between the pivots.

The graphs illustrate the experimental evolution of each pivot's trajectory over time. It is evident that the red pivot follows a nearly circular trajectory, while the green pivot exhibits a more erratic and unpredictable path. The black curve represents the difference between the green and red pivot trajectories, revealing an almost circular path, reflecting the relative motion between the two.

We have reduced the value of the smoothing window to 1 to achieve greater precision. Although it may appear less accurate, the results provide better and closer solutions.

```

1 % Apply a smoothing filter (e.g., moving average) to reduce motion blur
2 % effects
3 smooth_window = 1;
4 blue_positions = movmean(blue_positions, smooth_window, 1);
5 red_positions = movmean(red_positions, smooth_window, 1);
6 green_positions = movmean(green_positions, smooth_window, 1);

```

Angles:

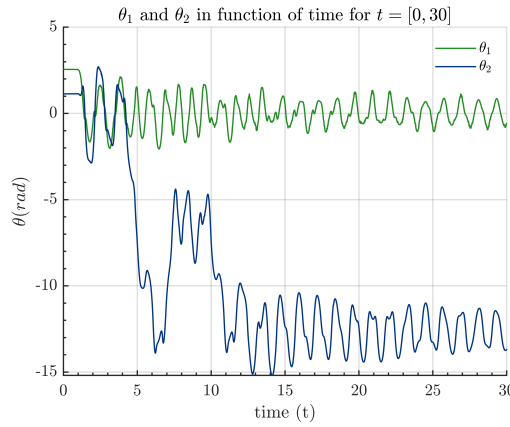


Figure 5: Evolution of θ_1 and θ_2 as a function of time.

The angular displacements θ_1 (green) and θ_2 (blue) show oscillatory behavior. Over time, θ_2 decays significantly, while θ_1 stabilizes near equilibrium. This decay reflects energy dissipation and loss of stability in θ_2 .

The reason our angles extend beyond the range $(-\pi, \pi)$ is that we have implemented a function to detect the jumps in the arctangent function and consecutively add or subtract them.

```

1 if delta_theta2 > pi
2     delta_theta2 = delta_theta2 - 2*pi;
3 elseif delta_theta2 < -pi
4     delta_theta2 = delta_theta2 + 2*pi;
5 end
6
7 theta1_cont(i,1) = theta1_cont(i-1) + delta_theta1;
8 theta2_cont(i,1) = theta2_cont(i-1) + delta_theta2;

```

Velocity and Energy:

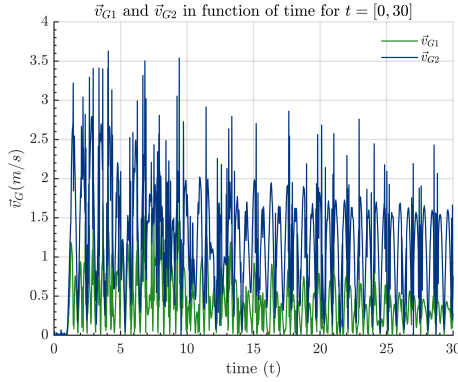


Figure 6: The velocity of the center of mass of each limb.

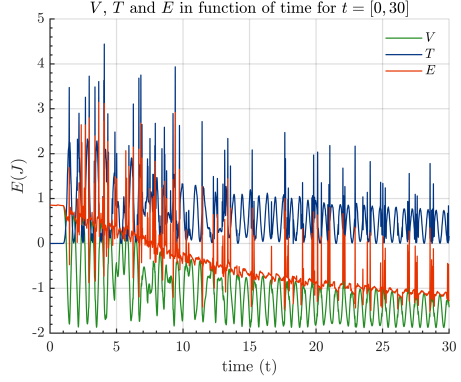


Figure 7: Theoretical kinetic, potential and total mechanical energy of the system.

The first graph (Figure 3) illustrates the velocities of the centers of mass, v_G^1 (green) and v_G^2 (blue), over time. v_G^2 exhibits significantly higher amplitudes and more chaotic behavior compared to v_G^1 , consistent with observations from the experimental setup. The velocity v_G^1 remains relatively small and stable, reflecting limited dynamic motion. On the other hand, the second graph (Figure 4) displays the evolution of potential energy V (green), kinetic energy T (blue), and total energy E (red) over time. Large oscillations at $t = 0$ indicate energy exchange between components. Over time, the total energy decays due to damping and friction, while the kinetic energy exhibits spikes corresponding to sudden accelerations.

7 Numerical Results:

Angles:

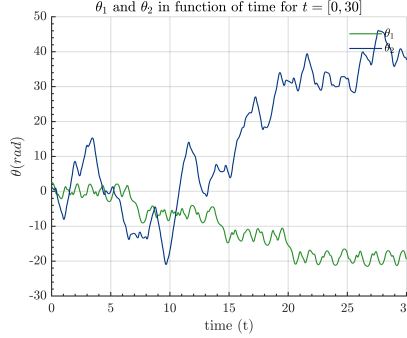


Figure 8: Numerical evolution of θ_1 and θ_2 as a function of time.

The figure illustrates the evolution of angles 1 and 2 as a function of time. As observed, angle 1 exhibits a progressive decay, while angle 2 shows fluctuating behavior over time. This fluctuation is attributed to the instability of the second rod.

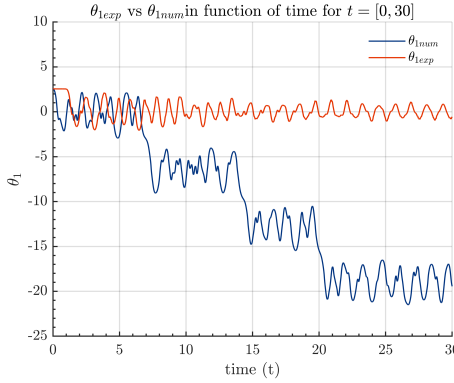


Figure 9: Numerical and Theoretical evolution of θ_1 .

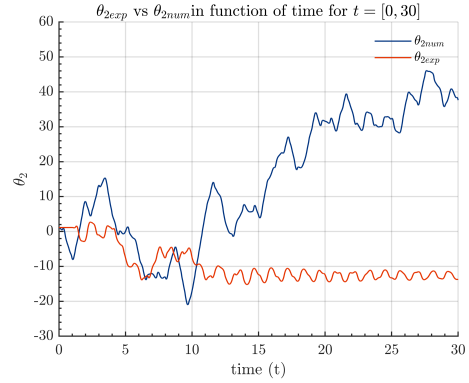


Figure 10: Numerical and Theoretical evolution of θ_2 .

The figure compares the theoretical and experimental values of angles 1 and 2 as a function of time. For angle 1, a significant discrepancy is observed between the two datasets, highlighting the influence of damping and frictional forces on the behavior of the first rod. In contrast, angle 2 shows an increasing trend in the experimental data, deviating from the expected decreasing behavior. This suggests a higher degree of randomness in the experimental performance than initially anticipated, further underlining the complexity of the system.

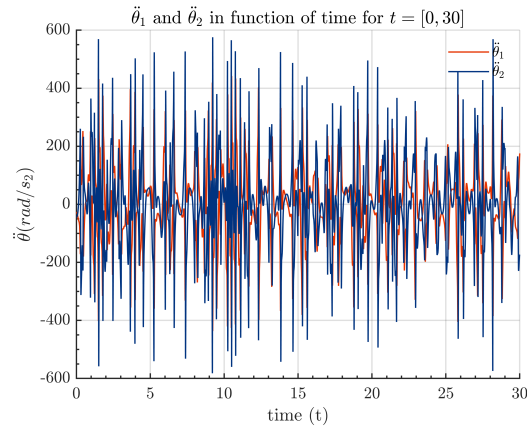


Figure 11: Evolution of $\ddot{\theta}_1$ and $\ddot{\theta}_2$ as a function of time.

The graph shows the angular acceleration as a function of time, highlighting its fluctuations around a consistent trend. It is noticeable that the data presented corresponds to both rods, which follow a similar pattern.

Phase Portraits:

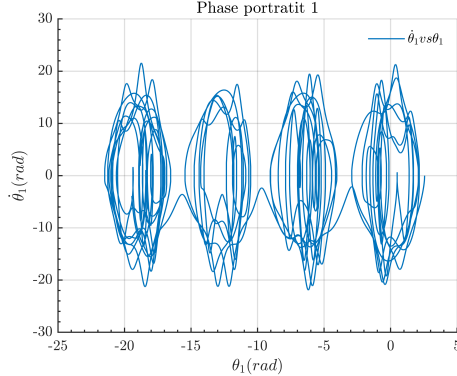


Figure 12: Phase portrait of $\dot{\theta}_1$ with respect to θ_1 .

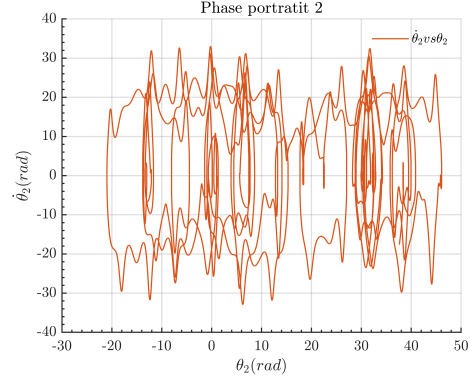


Figure 13: Phase portrait of $\dot{\theta}_2$ with respect to θ_2 .

The figures illustrate the evolution of the angular velocity of the rods as a function of the angle variation. It is evident that the graph corresponding to the first rod exhibits greater predictability compared to the second rod, whose motion is characterized by instability.

Theoretical and Numerical Pivot Positions:

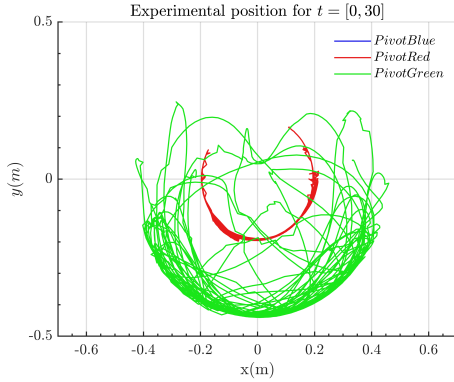


Figure 14: Experimental position of the three pivots in the x and y axis.

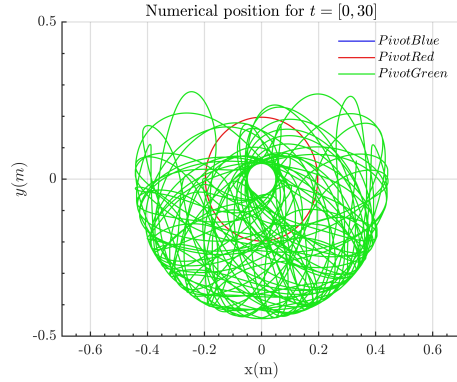


Figure 15: Numerical position of the three pivots in the x and y axis.

Both graphs depict the motion of the pivots, presenting the experimental and numerical values derived from the trajectory as a function of time. The kinematics based on the theoretical values demonstrate a predictable movement of the rods, whereas the experimental results deviate from the expected values. This discrepancy is due to the effects of damping and frictional forces, which influence the system and prevent it from following an idealized case.

Energies:

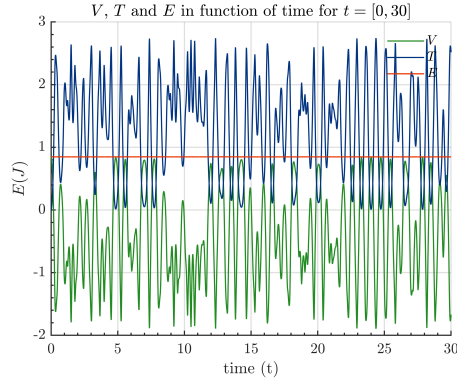


Figure 16: Numerical kinetic, potential and total mechanical energy of the system.

The figure illustrates the theoretical trend of energy conservation. While energy is expected to remain constant according to the theory, the experimental results, as previously discussed, reveal a different outcome due to the influence of external factors and system limitations.

PONCAIRE (EXTRA):

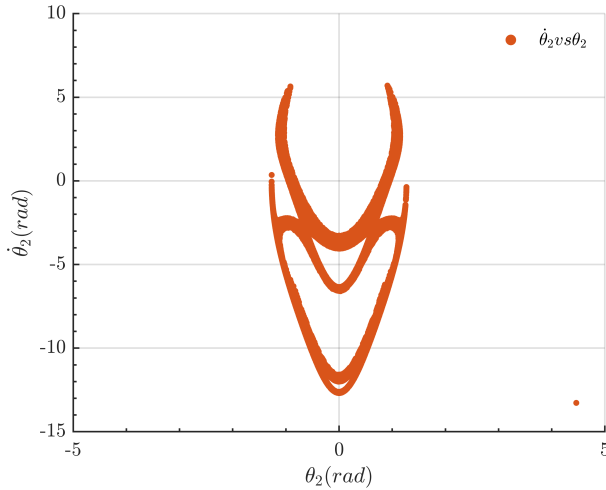


Figure 17: Evolution of θ_1 and θ_2 as a function of time.

We obtained the points of the Poincaré map by checking the sign change in θ_1 during iterations:

$$\theta_1(t_n) < 0 \quad \text{and} \quad \theta_1(t_{n-1}) > 0.$$

When this condition is satisfied, we compute the average of the angular positions and velocities for θ_2 as:

$$\bar{\theta}_2 = \frac{\theta_2(t_n) + \theta_2(t_{n-1})}{2}, \quad \bar{\dot{\theta}}_2 = \frac{\dot{\theta}_2(t_n) + \dot{\theta}_2(t_{n-1})}{2}.$$

```

1  for i = 1:n_iter
2
3      inicond= [theta1_sol(i), 0, theta2_sol(i), 0];
4      [t_p, X] = ode23s(@(t_p, X) ddiff_eq(t_p, X, g, L(1), m(1), m(2), I
5          (1), I(2), R(1), R(2)), tspan, inicond, Opt);
6
7      for j = 1:length(t_p)-1
8
9          if X(j,1) < 0 && X(j+1,1) > 0
10             poncaire_indices(a,1) = (X(j,3)+X(j+1,3))/2;
11             poncaire_indices(a,2) = (X(j,4)+X(j+1,4))/2;
12             a = a+1;
13         end
14
15     end

```

The image offers a comparison of the angular velocity of the second rod as a function of its angle variation. This comparison is generated by solving several differential equations, all maintaining the same initial energy but varying the initial conditions of the first rod. By employing this method, a detailed analysis of the second rod's behavior under different initial conditions is made possible, providing deeper insight into its dynamic response.

A Poincaré map is a powerful tool used in the analysis of dynamical systems, particularly for studying periodic orbits and the behavior of systems in a reduced, lower-dimensional space. It involves selecting a specific lower-dimensional subspace, often a plane or a curve, within the system's state space. The map then captures the points where the system's trajectory intersects this subspace, effectively transforming the continuous dynamics into a discrete sequence of points. This process allows for the visualization of the long-term behavior of the system, such as the identification of stable and unstable periodic orbits, and provides insights into the structure of attractors, bifurcations, and chaos. Poincaré maps are especially useful in complex systems where direct analysis of the full state space is challenging, offering a simplified yet insightful representation of the system's evolution.

8 Final Conclusion

The compound double pendulum experiment we studied for this session provided valuable insights into the dynamics of complex mechanical systems. Through experimental observation and numerical modelling, the behaviour of the pendulum was successfully characterized, and several key findings can be highlighted.

By recording the motion of the pendulum, the experimental data was collected. The positions of the pivot points were accurately extracted. This data provided the basis for determining the initial conditions $(\theta_1, \theta_2, \dot{\theta}_1, \dot{\theta}_2)$ for numerical simulations and allowed for direct comparison with the simulated motion. The equations of motion were derived and solved using the ode23s solver in MATLAB. While the kinematics closely matched the experimental data, the took a different road, as experimentally the energy was not conserved, albeit the numerical calculations showed the aforementioned should be conservative.

Overall, this experiment successfully combined theoretical, experimental and numerical analysis to provide a comprehensive understanding of a dynamic system. The findings illustrate the power of numerical methods in modeling complex systems and emphasize the importance of validating numerical results with experimental data.